Appl Phys B (2011) 105:649–657
DOI 10.1007/s00340-011-4699-5

Applied Physics B
Lasers and Optics

Ultra-high resolution optical coherence tomography for encapsulation quality inspection

J. Czajkowski · T. Fabritius · J. Ulański · T. Marszałek · M. Gazicki-Lipman · A. Nosal · R. Śliż · E. Alarousu · T. Prykäri · R. Myllylä · G. Jabbour

Received: 23 October 2010 / Revised version: 20 April 2011 / Published online: 28 August 2011

Abstract We present the application of ultra-high resolution optical coherence tomography (UHR-OCT) in evaluation of thin, protective films used in printed electronics. Two types of sample were investigated: microscopy glass and organic field effect transistor (OFET) structure. Samples were coated with thin (1–3 μm) layer of parylene C polymer. Measurements were done using experimental UHR-OCT device based on a Kerr-lens mode locked Ti:sapphire femtosecond laser, photonic crystal fibre and modified, free-space Michelson interferometer. Submicron resolution offered by the UHR-OCT system applied in the study enables registration of both interfaces of the thin encapsulation layer. Complete, volumetric characterisation of protective layers is presented, demonstrating possibility to use OCT for encapsulation quality inspection.

J. Czajkowski (✉) · T. Fabritius · R. Śliż · T. Prykäri · R. Myllylä · G. Jabbour
Optoelectronics and Measurement Techniques Laboratory, University of Oulu, P.O. Box 4500, 90014 Oulu, Finland
e-mail: jakub.czajkowski@ee.oulu.fi

J. Ulański · T. Marszałek
Department of Molecular Physics, Technical University of Łódź, 90-924 Łódź, Poland

M. Gazicki-Lipman · A. Nosal
Institute of Mechanical Engineering, Technical University of Łódź, 90-924 Łódź, Poland

E. Alarousu · G. Jabbour
Solar and Photovoltaics Engineering Research Center, King Abdullah University of Science and Technology, Thuwal, Jeddah 23955-6900, Saudi Arabia

1 Introduction

We are surrounded by numerous electronic and printed devices in our every day's life. Their presence is obvious for us and one is probably unable to picture a world without them. These devices get smaller and smarter all the time, while their lifetime is tailored to specific application. Nowadays, aside the chase for miniaturisation, researchers and developers work towards creation of the most robust, compact, and cost-effective devices possible.

In recent years, new materials and fabrication methods enabled production and application of new devices. An example is printed and flexible electronics, which is rapidly developing branch of the research and today's market. Organic field effect transistors (OFET), flexible organic solar cells (OPV), organic light emitting diodes and transistors (OLEDs and OLETs), as well as many other devices are under study in that field. There is a similarity between these devices: they contain organic materials. Such materials have great properties, but on the other hand require appropriate treatment and environment conditions to work as expected. Most of the organic materials need protection against humidity, oxygen, carbon dioxide etc. [1]. In addition, some of them require mechanical protection, which increases robustness of the device.

Thin protective films are used to secure proper operation conditions and to isolate the devices based on organic components from environment (and from each other). Such films are called encapsulation layers and are usually based on polymers. The thickness of these layers ranges from hundreds of nanometres to single micrometres.

As the lifetime of the device depends on the properties of encapsulation layer, inspection of its quality is extremely important. As Donaldson noted in 1996 [2], due to non-hermetic encapsulation paradigms it is very important for

adhesive bonding to exist at the interface between encapsulant and the components encapsulated. Only then the barrier is successful. This is the case with parylene C, for which the adhesion strongly depends on the substrate materials e.g., its adhesion to gold, platinum and silicon nitride is satisfactory, while the adhesion to polyimide is very low [3]. Hassler et al. presented adhesion measurements for parylene C using 90° peel, T-peel and tensile shear [4]. The tests presented are destructive and their applicability is rather limited to laboratory environment.

From an industrial point of view, in addition to adhesion, the uniformity, continuity and thickness of the layer are the obvious quality parameters for protective layers. Although polymers used for encapsulation are mostly optically transparent, it is difficult to evaluate their layers using visual methods, such as e.g., classical microscopy. One is not able to precisely assign the features to particular layer in the specimen's structure. Much more reliable and commonly used measurement technique is confocal microscopy (CM). It is able to provide highly accurate volumetric data and uses spatial rejection of out-of-focus light to improve resolution and contrast.

To analyse the quality of the encapsulation layer with other classical methods, complex or destructive techniques have to be applied. Atomic force microscopy (AFM) [1] or scanning electron microscopy (SEM) could be used to obtain detailed information on topography and quality of the surface. Microtomy or X-ray microscopy could provide information about the structure beneath that surface. Some groups studied coating layers' properties using surface insulation resistance, leakage current measurements [5, 6] or Fourier transformed infrared spectroscopy (FTIR) [6]. All this methods are either destructive, complex, expensive or do not provide point-by-point information about the encapsulation.

Optical coherence tomography (OCT) could be an alternative technique. OCT can be understood as an imaging modality based on the principles of low coherence interferometry (LCI). It is a mature technique, first presented by Huang et al. in 1991 [7]. Since then, many groups have studied its principles and applications. Most of the effort focused on bio-medical applications like e.g., ophthalmology. However, several non-medical applications have also been proposed [8–12]. When needed, the robustness of the OCT can be enhanced by combining it with CM in so called optical coherence microscopy (OCM) [13]. Such a combination adds improved depth resolution and sensitivity [14].

The study presented on the use of optical coherence tomography in encapsulation quality inspection was done within PolyNet research project—part of the European Community's Seventh Framework Programme (FP7/2007–2013). The idea behind such application of OCT is based on the principles of low coherence interferometry and its sensitivity for refractive index changes. Whenever there is a defect in the encapsulation layer it could be seen, either by a change of the number of peaks in the interference fringe signal envelope, or as a change in the signal amplitude. Such an amplitude change corresponds to the refractive index mismatch at the interface between materials. The authors assume that one should be able to create an encapsulation map, indicating place, size, and exact shape of defects in the protective layer.

2 Measurement system

Measurements presented in this study were done using experimental, ultra-high resolution, time domain optical coherence tomography system (UHR-OCT) developed at the University of Oulu [10, 11, 15, 16]. To achieve ultra-high axial resolution, broadband i.e., low coherent light source has to be used. Detailed discussion of the resolution and other key technological parameters of the OCT can be found in review paper presented by Drexler in 2004 [17].

In our UHR-OCT system a Kerr-lens mode locked Ti-sapphire femtosecond laser is followed by a photonic crystal fibre (PCF). Due to the very broad spectrum of such light source, our system is based on the modified free-space Michelson interferometer. The measurement process is controlled by specially developed LabVIEW™ program [18]. Detailed layout scheme of the developed system can be seen in Fig. 1.

The OCT system uses the TISSA-50 (CDP Corp., Russia) femtosecond laser. It generates <50 fs pulses with the centre wavelength around 800 nm. After the laser cavity, light propagates through the Faraday's isolator to prevent feedback from the interferometer. After the isolator light travels through dispersion compensation path consisting of two prisms and two mirrors. Corrected beam is then coupled into a photonic crystal fibre (PCF, Femtowhite 800, NKT Photonics, Denmark) and is broadened in so called supercontinuum generation process. High output power (around 130 mW after the PCF) and bandwidth ranging from 400 to 1700 nm enables sub-micron axial resolution [10, 16]. The results presented by other research groups prove the concept of submicron OCT imaging [19–21].

The A-scan (i.e. the depth scan) is acquired by movement of piezoelectric scanner in the reference arm (P-783, Physik Instrumente, Germany). The scanner is fitted with a mirror and a focusing lens. To keep both interferometer arms in focus during the measurement, another piezoelectric scanner is used in the measurement arm. Various dynamic focusing schemes can be utilised. For the measurements presented the piezoelectric scanner in the measurement arm was operated in a slave mode for the scanner in the reference arm. The lenses used in the system are achromatic doublet with the

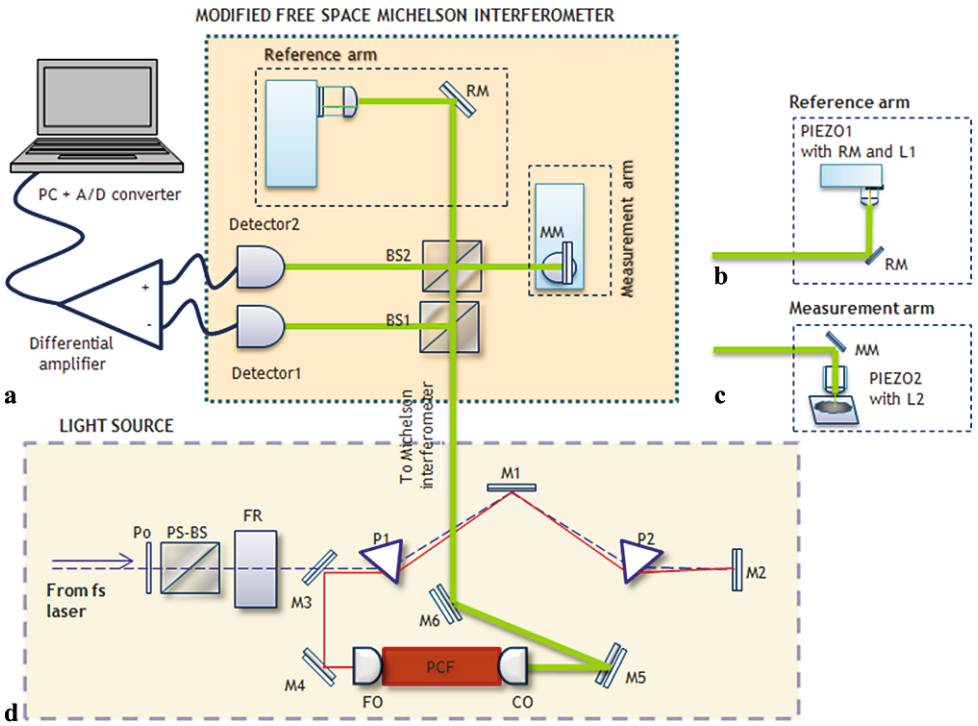

Fig. 1 Layout scheme of the experimental UHR-OCT device. (**a**) Michelson type interferometer: *BS1*, *BS2*: beam splitters, *RM*: reference mirror, *MM*: measurement mirror, *L1–L2*: focusing lenses. (**b**) reference arm, (**c**) measurement arm, (**d**) light source for the interferometer: *Po*: polariser, *PS–BS*: polarisation sensitive beam splitter, *FR*: Faraday's rotator, *P*: prisms for dispersion compensation, *M*: mirror, *Fo*: focusing objective, *Co*: collimation objective

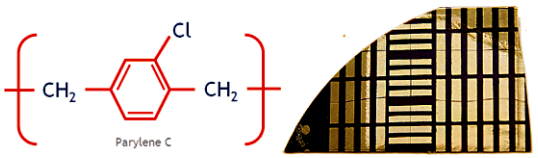

Fig. 2 Chemical scheme of parylene C (*left*) and coated OFET structure used in presented study (*right*)

focal length of 25 mm. For the collimated beam of 10 mm in diameter the numerical aperture of the lenses equals 0.196. Lateral scanning is done using two stepper motor stages controlled by ESP300 driver (Newport, USA).

Due to the use of time domain OCT method and the adjustable femtosecond laser, a balanced detector is employed to ensure a high SNR ratio (PDB150A-EC, Thorlabs, Germany). Following the measurement, analogue signal is filtered, digitised and further processed using Matlab and ParaView software.

3 Analysed samples

Special barrier properties make parylene C (Fig. 2) eligible for the conservation applications [1, 22]. It is also known that parylene C layers can also find application in the field of organic large area electronics (OLAE)—as the support [23] or as the dielectric layer [23, 24].

In our case, all samples of parylene C were evaporated by chemical vapour deposition (CVD) [25]. The deposition process starts from a dimer (dichloropara-xylylene), which decomposes during heating to form a gaseous monomer (chloropara-xylylene). Then the monomer gas flows into a deposition chamber containing the object to be coated. A solid polymer layer (polypara-xylylene) is obtained from the monomer gas, which condenses and polymerises on each surface of the object placed in the chamber.

3.1 Microscopy glass

In the first step a 2 μm thin film of parylene C was deposited on the previously cleaned glass plate. This sample was treated as the reference. The second sample was prepared by removing previously deposited parylene C film from the glass plate and by putting it again. Another sample was fabricated using a situated lubricant on the glass before parylene deposition process and by heating it afterwards in air conditions. This allowed for formation of artificial gas chambers below the polymer layer.

3.2 Organic field effect transistors (OFETs)

In the fabrication process of the OFET device (Fig. 2) a semiconductor layer parylene derivative PTCDI-C5(3) (SynTec GmbH Wolfen) was used. Highly oriented polycrystalline films of PTCDI-C5(3) were prepared by zone-casting technique [26] on silicon (Si) wafers with thermally

grown, 150 nm thick, silicon dioxide (CEMAT Silicon). The FET devices based on perylene derivatives were fabricated in the top contacts–bottom gate configuration. Aluminium source and drain contacts were vacuum evaporated on the top of PTCDI-C5(3) layers. All devices were covered by 1 μm thin parylene C films.

4 Measurements and results

4.1 Measurement principle and typical data processing

The study presented on the encapsulation quality inspection began with the hypothesis based on the properties of low coherence interferometry. In LCI, a low coherent beam is coupled into the interferometer and split into a reference and a probing beam. The probing beam is then focused on the analysed sample. Light is scattered and comes back to the interferometer. It interferes with the reference beam creating fringe signal, which contains structural information about the measured specimen. Such fringe signal acquired from a single lateral point is commonly referred to as an A-scan or simply a depth scan. By combining several A-scans together, side by side, one is able to create a tomogram, commonly known as a B-scan (Fig. 3).

The initial hypothesis of presented study states that: presence of voids, impurities, and problems with adhesion of encapsulation layer, causes refractive index mismatch, which in turn affects the local amplitude of the interference fringe signal. Each A-scan acquired during the measurement can be treated as superposition of depth dependent reflectance. Therefore, to some degree, defects could be recognised even when their size in depth is smaller than the axial resolution offered by the OCT device.

Computational processing algorithm was implemented to get more detailed information about the encapsulation quality. In the first of step, depth position of the encapsulation layer's surface is resolved using thresholding. The level for the thresholding algorithm is chosen based on the amplitude of the interference peak corresponding to the surface of the analysed specimen. The operation is repeated for each A-scan within the volume and a surface topography map is created. The topography map is then low-pass filtered to discard possible errors e.g., caused by the excess noise or incorrect threshold level. Filtered topography map is used to specify a vertical region of interest

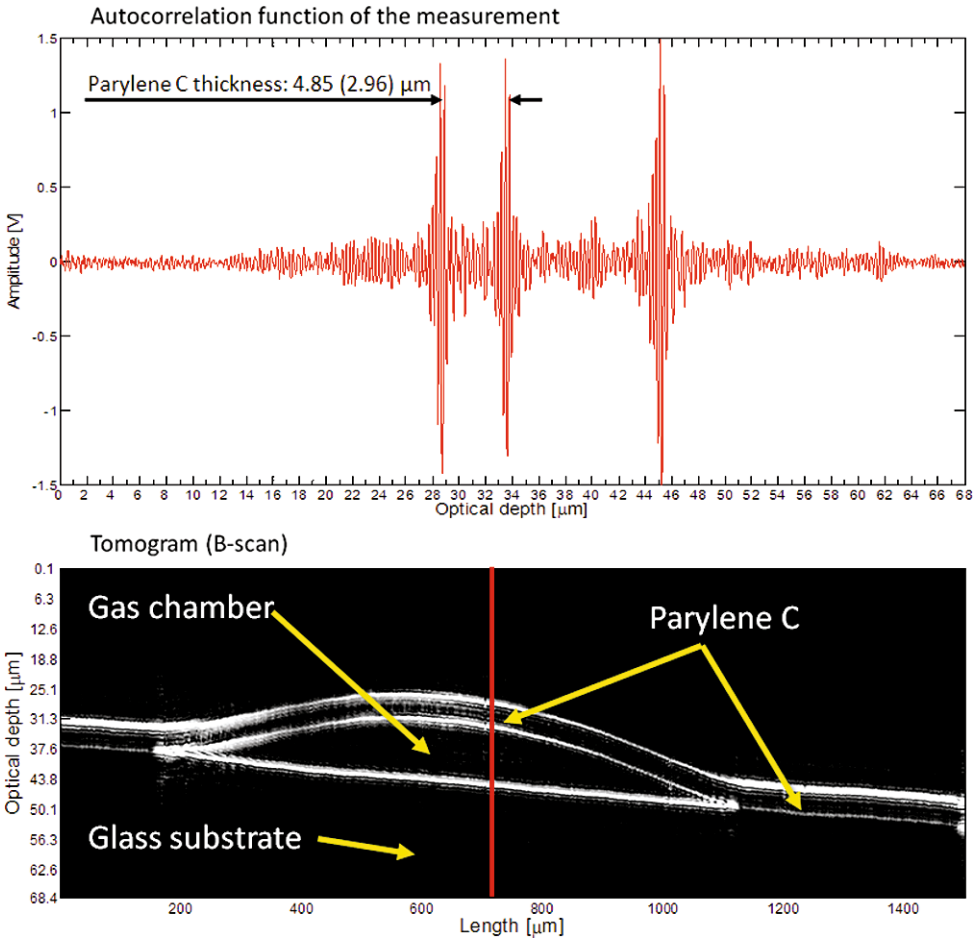

Fig. 3 Example A-scan of parylene C coated microscopy glass (*atop*). Thickness of parylene C in bracket given as physical (refractive index of parylene C was assumed to be 1.639). B-scan image (*below*) shows the place of origin for the A-scan profile (*marked with red line*)

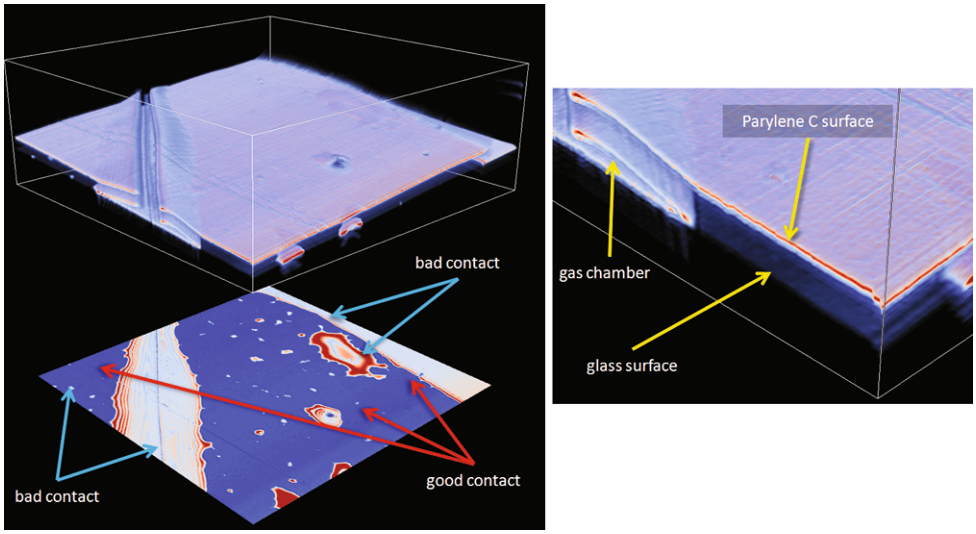

Fig. 4 Volumetric reconstruction of the parylene C coated microscopy glass (*left, atop*) and calculated amplitude map of the parylene C–glass interface (*left, bottom*). Boundary box indicates the size of the volume $2000 \times 2000 \times 208$ µm. Zoom-in image (*right*). Coating defects and gas chambers are clearly visible

(ROI) around the interface between encapsulant and protected structure.

Having the region of interest, the highest amplitude point and its depth index are calculated within the ROI's boundaries and an amplitude map of the interface is created. The map can be presented "as is" or further processed to simplify its evaluation (e.g., using binarization algorithms). Topography map of the interface is saved for further reference. In order to get more reliable information about encapsulation quality, a thickness of the encapsulation layer is calculated by subtracting the surface topography map from the encapsulant-substrate interface topography map.

4.2 Preliminary tests with microscopy glass

To test the hypothesis a microscopy glass coated with thin, 2 µm layer of parylene C was analysed. Area of 2×2 mm was measured using UHR-OCT system with 5 µm lateral measurement step. Axial range of the measurement 208 µm was limited by the scanning distance of the piezoelectric scanner in the reference arm of the interferometer.

The amplitude map, obtained from the measurement data can be seen in Fig. 4. As expected, regions of higher amplitude can be clearly seen. For comparison, Fig. 4 contains also a complete, volumetric reconstruction of the specimen. Artificial gas chambers located under the polymer layer are clearly visible and correspond well with calculated amplitude map. Moreover, amplitude map reveals defects, which are not clearly visible when viewing sample's surface (e.g., the big feature on the right side of the map).

4.3 Functional device analysis—organic field effect transistors (OFETs)

To extrapolate the hypothesis more complex or real-life specimen should be used. Such requirements were met by organic field effect transistor (OFET) structures, covered with 1 µm thin layer of parylene C. Area of 2×2 mm was measured with 5 µm transversal steps. Depth range of the measurement was 73 µm. Ultra high resolution offered by our OCT system enabled us to resolve both interfaces of the polymer layer. Moreover, interfaces of this 1–2 µm thin layer were successfully acquired over the whole measured volume being one of the smallest feature sizes measured with OCT ever.

The amplitude map of the parylene C–OFET interface was calculated with the algorithm described above. The map and corresponding volumetric reconstruction of the OFET structure can be seen in Fig. 5.

According to our hypothesis, one would expect to see regions of higher amplitude indicating the presence of defects. However, in the case of OFET measurement things were slightly different. Instead of simple "good-bad" amplitude pattern one could see places of significantly lower amplitude.

Observing the pattern in the amplitude map one could assume that the reason for the presence of low-amplitude areas comes from the roughness of the interfaces. The idea behind such assumption is quite simple. The light scattered or reflected by the sample has to be coupled back into the interferometer. In case of rough samples, sharp edges, and features inclined to optical axis of the interferometer at large angles, the probing beam may be reflected away. In case of presented OFETs, the surface roughness originates from the crystalline nature of PTCDI-C5 and silicon. The feature size is then much below the axial resolution of the UHR-OCT device. Despite that fact, surface structure still affects the amplitude map.

To analyse the correlation between the amplitude map and local roughness, topography of the parylene C layer (i.e., surface of the sample) was studied. The local roughness

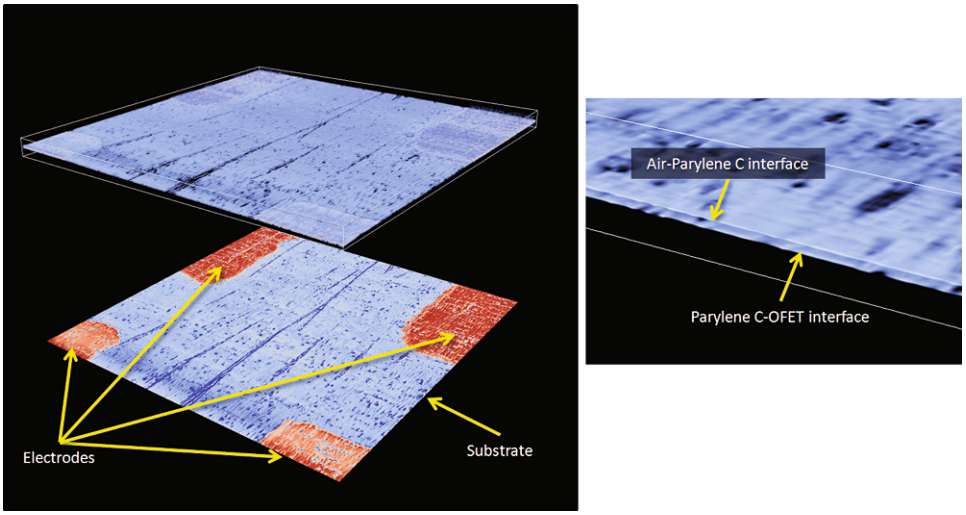

Fig. 5 Volumetric reconstruction of the parylene C coated OFET structure (*left, atop*) and calculated amplitude map of the parylene C–substrate interface (*left, bottom*). Boundary box indicates the size of the volume $2000 \times 2000 \times 73$ µm. Zoom-in image showing interfaces of 2 µm thin polymer layer (*right*)

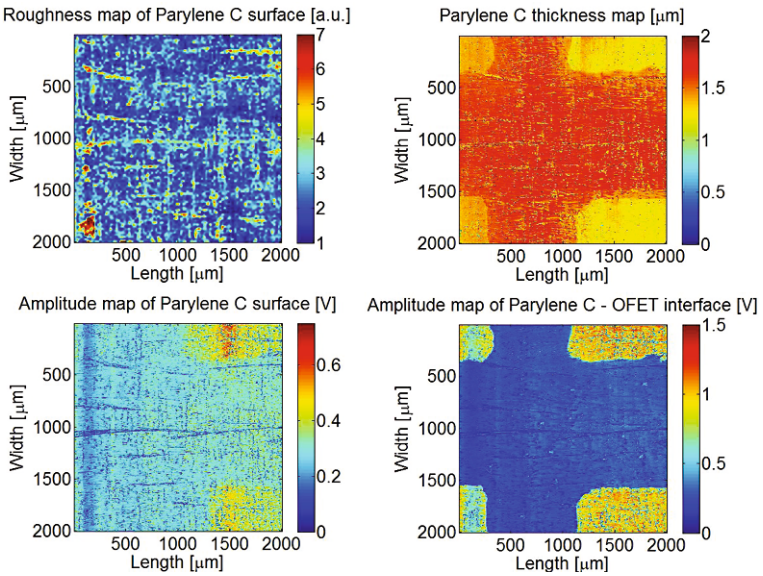

Fig. 6 First measurement of the OFET structure. Local roughness map of the parylene C surface calculated with 4×4 point kernel (*left atop*), thickness map of the parylene C layer (*right atop*), amplitude map of the parylene C surface (*left bottom*), and amplitude map of the OFET surface (*right bottom*)

was calculated by dividing the surface into 4×4 pixel subsurfaces and calculating Ra roughness parameter for each of them (mean roughness [27]). Calculated parameters create a pixel in the local roughness map. The map can be seen in Fig. 6 presenting also the amplitude maps of both: parylene C and OFET surfaces and a thickness map of the encapsulant. Despite four times lower resolution caused by the roughness calculation procedure, clear correspondence between amplitude and roughness maps can be observed. Therefore, the hypothesis based on amplitude alone has limited application in case of samples with highly rough surfaces or samples with varying roughness.

Nevertheless, OCT is able to resolve full volumetric structure of analysed specimen. In case of the OFET structure, the best way to evaluate the quality of protection layer could be either 3D rendering as presented in Fig. 5, or calculation and analysis of the thickness map. Such approach has additional assets. As discussed in the introduction, quality of encapsulation layer is not only related to the adhesion properties of the layer, but also to its thickness and uniformity. An example parylene C thickness map for the OFET sample can be seen in Fig. 6. Due to the presence of electrodes and due to surface features of the substrate, one can observe places of lower thickness. However, only few places of thickness lower than 1 µm were registered. Furthermore, overall thickness is slightly higher than expected from the deposition process' parameters.

4.4 Additional tests and reference measurements

To be able to exclude possible measurement error affecting amplitude of the interference signal, additional measurement of OFET structure was done after realignment of the OCT system. In this measurement, an area of 4×1 mm was

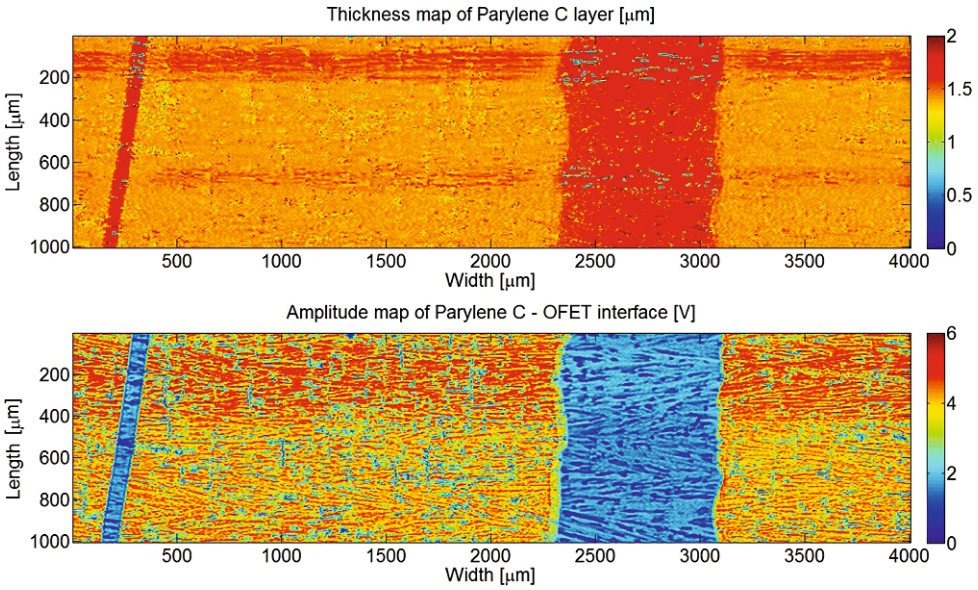

Fig. 7 Second measurement of the OFET structure. Thickness map of the parylene C layer (*atop*) and amplitude map of the OFET surface (*bottom*)

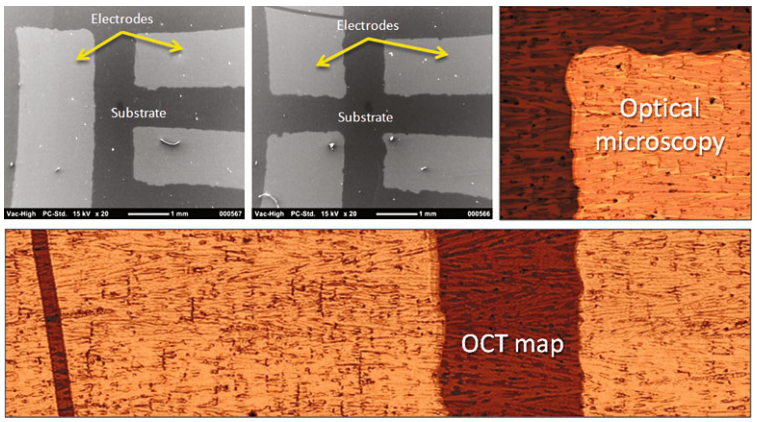

Fig. 8 Image acquired during the SEM measurement (*left and middle, atop*), image obtained with the optical microscope (*right, atop*), and amplitude map calculated from the OCT measurement data (*bottom*)

studied. As before, also in this case, the amplitude map of encapsulant-substrate interface was calculated. Again, the artifacts could be observed and were in good correlation with local roughness of the layer. Thickness map of the polymer layer and amplitude map of the OFET surface are presented in Fig. 7. Thickness of the layer seems to be uniform and only few places yield lower values. One can see two horizontal regions of higher values caused by temporary, unstable regime of the femtosecond laser. Since the thickness map reveals no significant anomalies, the authors assume no defects in the encapsulation layer. Moreover, no gas chambers were registered. The authors therefore presume that the presence of such defects would still be reflected in the amplitude maps.

To investigate the surface of the polymer layer, scanning electron microscope (SEM) and optical microscope were used. Figure 8 shows the results of SEM and optical microscopy measurements, as well as amplitude map calculated from the OCT measurement (custom colour map is used to emphasise similarities). In the SEM measurement, performed with JEOL Neoscope JCM-5000 (JEOL, Japan), no surface structure could be seen. Such behaviour could be explained by the non-conductive nature of the polymer. To resolve the structure, sample should be coated with a layer of conductive material e.g., gold. It renders such evaluation technique as destructive and unpractical from industrial point of view.

Although optical microscopy (Eclipse LV100DA-U, Nikon, Japan) revealed the same kind of pattern, as the one observed in the OCT amplitude map, it is not able to provide information about the quality of the encapsulation layer. In addition to difficulty of assigning features in the image to particular layers, it is also not possible to justify the adhesion of the encapsulation layer. Therefore, optical microscopy cannot be considered as a competitive technique to OCT in encapsulation quality inspection. However, the similarity between the images had the effect of giving us an idea on how to compensate for signal loss in OCT amplitude maps. To do so, one could correlate the amplitude map of the interface below the encapsulation layer with an

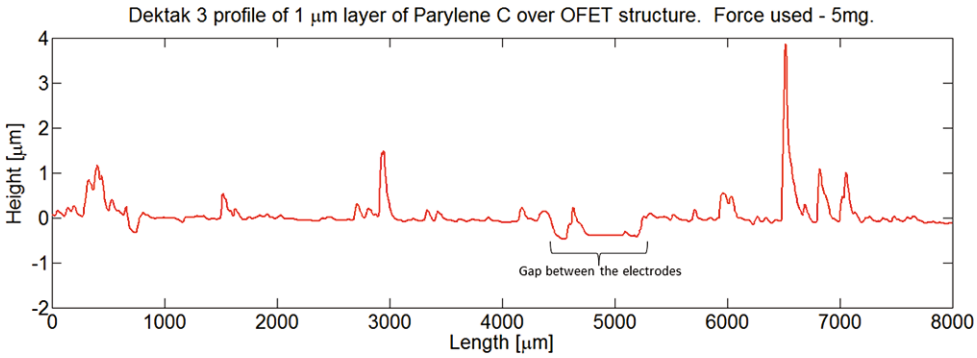

Fig. 9 Reference profile obtained with Dektak 3 stylus profiler. Force used in the measurement equalled 5 mg

amplitude map of the polymer's surface to justify signal losses.

To verify our assumptions concerning the surface roughness of the OFET samples, one more reference measurement was done. Dektak 3 (Veeco, USA) stylus profiler was used. One, 8 mm long profile was measured along the direction of the OFET electrode. The profile obtained shows several sharp features rising from the surface of the polymer layer. A gap between electrodes i.e. the area of bare substrate can be clearly identified. Results can be seen in Fig. 9.

The layer of parylene C over the OFET structure was obtained in chemical deposition process. Therefore it can be treated as uniform in thickness. Such assumption means that the size of features at the surface of the polymer corresponds to the size of features beneath the layer. As expected, the mean size of the surface features of the OFET structure is small when compared with the axial resolution offered by state of the art OCT systems. For the profile of 1600 points the obtained the Ra roughness parameter yields 186.1 nm, while Rq (the RMS roughness [27]) equalled 354.2 nm.

5 Conclusion

The study presented shows perspective for the application of optical coherence tomography in quality inspection of encapsulation layers. This perspective involves an extremely fast growing branch of electronics i.e., printed, flexible and organic electronics.

Efficient and accurate characterisation techniques are highly demanded on today's market. From manufacturers' point of view, there is a strong need for cost reduction and quality improvement at the same time. For electronics based on organic materials, encapsulation is one of the key processes aiming to fulfil these requirements. Encapsulation layers used to isolate the final product from the outside environment are to play a great role in the fabrication process and guarantee a proper lifetime of the device. On the other hand, the layers are thin (single micrometres in thickness), mostly optically transparent, non-conductive, and not so resistive to mechanical measurement techniques. Therefore, optical coherence tomography could be a potential solution. The benefits offered by the OCT when applied to quality inspection include: no need for sample preparation, non-contact and non-destructive measurement manner, high volumetric accuracy, short measurement times and flexibility of the technique. To enhance its sensing parameters OCT could be combined with confocal microscopy creating a great characterisation tool.

As in the other articles, also here the authors would like to draw the reader's attention to the great progress that took place during the recent years in OCT. The light sources become cheaper, broader and more compact. Similarly, new signal acquisition schemes and new types of detector decreased measurement time dramatically.

Nowadays, the most widely used OCT systems are based on Fourier/spectral domain approach. They offer high measurement speed and high axial measurement resolution. These systems employ either very fast and accurate spectrographs (SD-OCT) [28] or tuneable laser sources (SS-OCT) [29]. Stretched pulse OCT systems offer even higher measurement speed, at the cost of lower axial measurement resolution [30, 31]. To the authors' best knowledge, no supercontinuum based, sub-micron resolution spectral domain OCT systems have been reported thus far.

In the near future, the UHR-OCT setup used in this study will be updated with a spectral domain detection mode. High speed spectrograph, employing CMOS camera and diffraction grating will be used for detection. Combined with our very broadband light source, it will hopefully allow for both great increase in measurement speed and conservation of the measurement resolution. Such an improvement renders UHR-OCT an even more attractive characterisation technique.

One could point out the high price of the Ti-sapphire crystal based femtosecond oscillators. However, an alternative exists on today's market. At least two companies offer integrated supercontinuum light sources based on femtosecond fibre lasers and photonic crystal fibres. The prices of such devices are much lower than for traditional oscillators;

however, the authors do not have knowledge of their stability and noise properties.

This study started with the initial hypothesis concerning the use of amplitude maps to justify encapsulation quality. Despite the fact that the hypothesis has not been fully confirmed, the authors have proved that UHR-OCT could be effectively used in encapsulation quality inspection. Ultra high resolution offered by our OCT system allowed us to measure <3 μm thin polymer layers and justify their properties. Problems that occurred during measurement data evaluation have been studied by both theoretical analysis and reference measurements. Possible solution scenarios have been proposed.

In case of all OCT measurements, data analysis requires prior knowledge about the expected specimen's structure and properties of the materials used in its fabrication process. With that information, optical coherence tomography is able to deliver highly accurate volumetric data of physical parameters and quality of the encapsulation layer.

Acknowledgements Presented study was done within PolyNet project and has been funded from the European Community's Seventh Framework Programme (FP7/2007-2013) under the grant agreement No. 214006. In addition, the authors would like to thank the Academy of Finland for the support in their research on UHR-OCT.

References

1. H. Lee, J. Cho, in *Proc. 2005 ASME Intl. Mech. Eng. Cong. Expo., IMECE* (2005), p. 82955
2. P.E.K. Donaldson, Int. J. Adhes. Adhes. **16**, 105 (1996)
3. T. Stieglitz, Microsyst. Technol. **16**, 723 (2010). doi:10.1007/s00542-009-0988-x
4. C. Hassler, R.P. von Metzen, P. Ruther, T. Stieglitz, J. Biomed. Mater. Res., Part B, Appl. Biomater. **93B**, 266 (2010). doi:10.1002/jbm.b.31584
5. J. Wu, R.T. Pike, C.P. Wong, N.P. Kim, M.H. Tnielian, IEEE Trans. Adv. Packaging **23**, 721 (2000). doi:10.1109/6104.795854
6. T. Stieglitz, in *Proc. 10th Annu. Conf. Intl. FES Soc.* (2005)
7. D. Huang, E.A. Swanson, C.P. Lin, J.S. Schuman, W.G. Stinson, W. Chang, M.R. Hee, T. Flotte, K. Gregory, C.A. Puliafito, Science **254**, 1178 (1991). doi:10.1126/science.1957169
8. D. Stifter, Appl. Phys. B **88**, 337 (2007). doi:10.1007/s00340-007-2743-2
9. P. Targowski, B. Rouba, M. Góra, L. Tymińska-Widmer, J. Marczak, A. Kowalczyk, Appl. Phys. A **92**, 1 (2008). doi:10.1007/s00339-008-4446-x
10. J. Czajkowski, T. Prykäri, E. Alarousu, J. Palosaari, R. Myllylä, Opt. Rev. **17**, 257 (2010). doi:10.1007/s10043-010-0045-0
11. T. Prykäri, J. Czajkowski, E. Alarousu, R. Myllylä, Opt. Rev. **17**, 218 (2010). doi:10.1007/s10043-010-0039-y
12. T. Fabritius, R. Myllylä, S. Makita, Y. Yasuno, Opt. Express **18**, 22859 (2010). doi:10.1364/OE.18.022859
13. J.A. Izatt, M.R. Hee, G.A. Owen, E.A. Swanson, J.G. Fujimoto, Opt. Lett. **19**, 590 (1994)
14. A.Gh. Podoleanu, R.G. Cucu, J.A. Rogers, J. Pedro, G. Dobre, M. Gomez, H. Liang, B.T. Amaechi, S. Higham, in *Proc. SPIE* (2007), p. 67851I. doi:10.1117/12.757868
15. E. Alarousu, T. Prykäri, J. Palosaari, R. Myllylä, in *Proc. 5th ODIMAP* (2006), pp. 210–215
16. T. Prykäri, E. Alarousu, J. Kuivaniemi, J. Czajkowski, R. Myllylä, in *Proc. 2nd Int. Top. Meet. Opt. Sens. AI Vision–OSAV'2008* (2008), pp. 111–117. ISBN:978-5-7577-0333-6
17. W. Drexler, J. Biomed. Opt. **9**, 47 (2004). doi:10.1117/1.1629679
18. P. Hosek, T. Prykäri, E. Alarousu, R. Myllylä, J. Assoc. Lab. Autom. **14**, 59 (2009). doi:10.1016/j.jala.2008.05.007
19. B. Povazay, K. Bizheva, A. Unterhuber, B. Hermann, H. Sattmann, A.F. Fercher, W. Drexler, A. Apolonski, W.J. Wadsworth, J.C. Knight, P.St.J. Russell, M. Vetterlein, E. Scherzer, Opt. Lett. **27**, 1800 (2002). doi:10.1364/OL.27.001800
20. J. Gong, B. Liu, Y.L. Kim, Y. Liu, X. Li, V. Backman, Opt. Express **14**, 5909 (2006). doi:10.1364/OE.14.005909
21. X. Ping, J.G. Fujimoto, Chin. Sci. Bull. **53**, 1963 (2008). doi:10.1007/s11434-008-0235-3
22. D. Feili, M. Schuettler, T. Doerge, S. Kammer, T. Stieglitz, Sens. Actuators A **120**, 101 (2005). doi:10.1016/j.sna.2004.11.021
23. R. Pfattner, M. Mas-Torrent, I. Bilotti, A. Brillante, S. Milita, T. Marszalek, J. Ulanski, A. Nosal, M. Gazicki-Lipman, M. Leufgen, G. Schmidt, V. Laukhin, J. Veciana, C. Rovira, Adv. Mater. **22**, 4198 (2010). doi:10.1002/adma.201001446
24. J. Jakabovic, J. Kovac, M. Weis, D. Hasko, R. Srnanek, P. Valent, R. Resel, Microelectron. J. **40**, 595 (2009). doi:10.1016/j.mejo.2008.06.029
25. A. Nosal, A. Zydorczyk, A. Sobczyk-Guzenda, L. Głuchowski, H. Szymanowski, M. Gazicki-Lipman, J. Achiev. Mater. Manuf. Eng. **37**, 442 (2009)
26. T. Marszałek, E. Dobruchowska, J. Jung, J. Ulański, M. Melucci, G. Barbarella, Eur. Phys. J. Appl. Phys. **51**, 33208 (2010). doi:10.1051/epjap/2010107
27. E.P. Degarmo, J.T. Black, R.A. Kohser, *Materials and Processes in Manufacturing*, 9th edn. (Wiley, New York, 2003). p. 223. ISBN:0-471-65653-4
28. I. Grulkowski, M. Gora, M. Szkulmowski, I. Górczyńska, D. Szlag, S. Marcos, A. Kowalczyk, M. Wojtkowski, Opt. Express **17**, 4842 (2009). doi:10.1364/OE.17.004842
29. R. Huber, D.C. Adler, J.G. Fujimoto, Opt. Lett. **31**, 2975 (2006). doi:10.1364/OL.31.002975
30. S. Moon, D.Y. Kim, Opt. Express **14**, 11575 (2006). doi:10.1364/OE.14.011575
31. Y. Park, T.-Y. Ahn, J.-C. Kieffer, J. Azana, Opt. Express **15**, 4597 (2007). doi:10.1364/OE.15.004597